

LASER TECHNOLOGIES

https://doi.org/10.1070/QEL16510

Low-coherence interferometry as a tool for monitoring laser micro- and nanoprocessing of diamond surfaces

V.V. Kononenko, E.V. Bushuev, E.V. Zavedeev, P.V. Volkov, A.Yu. Luk'yanov, V.I. Konov

Abstract. **We have demonstrated the possibility of using low-coherence tandem optical interferometry for monitoring the local laser processing of diamond surfaces. Noncontact measurements of the optical thickness of single-crystal diamond plates were performed directly during the exposure of the surface to repetitive intense laser pulses. We investigated the dynamics of the thinning of a single crystal in two radically different regimes of laser etching: ablation (KrF excimer laser, λ = 248 nm, τ = 20 ns) and nanoablation (Ti : sapphire laser, λ = 266 nm, τ = 100 fs).**

Keywords: *diamond, laser ablation, laser nanoablation, low-coherence interferometry.*

1. Introduction

Recent advances in chemical vapour deposition technologies have made it possible to produce synthetic single-crystal diamond plates having dimensions and quality sufficient for the fabrication of not only photonic [1–5] but also (in the long run) quantum devices [6–9]. Precision technologies for the micro- and nanoprocessing of diamond surfaces are among the key elements necessary for the development of diamond photonics and will determine its practical capabilities in the future [10]. This underlies the long-time research interest in laser-induced processes in diamond, sufficiently diverse and effective from the viewpoint of the controlled and fast processing of this extremely hard and chemically inert crystalline material.

At present, two technologically important processes can be distinguished, which can be initiated by appropriate laser irradiation. One of them is classic evaporative ablation, which is accompanied by diamond surface graphitisation and characterised by a relatively high material removal rate (above 10 nm per pulse) [11–15]. The other process on the diamond surface occurs when the laser fluence does not exceed the graphitisation threshold. In such a case, etching does not stop, but the etch rate decreases drastically, to below 10^{-3} nm per pulse, suggesting that this regime can be referred to as nanoablation [16, 17]. Basically, nanoablation is photostimulated diamond surface oxidation, a process that requires oxygen and yields volatile carbon oxides as products. In recent years, there has been increased interest in nanoablation processing because it has been shown that the associated surface photochemical reaction leads to the generation of surface vacancies, which then diffuse into the bulk of the crystal and react with substitutional nitrogen to form nitrogen–vacancy complexes (NV centres) [18].

Both described processes (ablation and nanoablation) require noncontact online monitoring techniques that would allow one to control irradiation and obtain a structure with tailored parameters (amount of removed material, density of defects produced in the surface layer, etc.) in the laser irradiation zone. Among the methods that hold the greatest promise for this purpose are those utilising interference, because they allow for real-time surface topography monitoring. However, the use of conventional coherence interferometry in both the ablation and nanoablation diamond processing regimes has a number of limitations. Ablation leads to a considerable increase in surface roughness, complicating measurements. It is also difficult to obtain relevant data if the material removal rate (per pulse) exceeds a value in the order of the incident light wavelength. In the case of nanoablation, a key problem is to ensure ultrahigh accuracy in measurements of the laser etch depth, which should be 1 nm or better. In this paper, we examine the feasibility of obviating the above problems using low-coherence fibre-optic interferometry, which was already utilised to monitor the laser macroprofiling of diamond [19].

2. Experimental

Figure 1 shows a schematic of the experimental setup used. For diamond plate surface processing in the ablation regime, we used a CL-7100 KrF excimer laser (Optosistemy) generating 248-nm pulses of duration τ = 20 ns. The laser pulse energy was 200 mJ and the pulse repetition rate was 50 Hz. The laser beam illuminated a square mask, and its image was projected onto the diamond surface in the form of a uniformly illuminated spot 40 × 40 μm in dimensions.

The laser system for etching diamond in the nanoablation regime included a Tsunami Ti : sapphire oscillator (Spectra Physics) and Spitfire regenerative amplifier (Spectra Physics), which generated 800-nm pulses with τ = 120 fs. After frequency tripling, the 266-nm laser light was focused onto the sample surface by a spherical lens with a focal length of 100 mm. The 1/e beam waist diameter was then ~10 μm.

V.V. Kononenko, E.V. Zavedeev, V.I. Konov A.M. Prokhorov General Physics Institute, Russian Academy of Sciences, ul. Vavilova 38, 119991 Moscow, Russia; National Research Nuclear University 'MEPhI' (Moscow Engineering Physics Institute), Kashirskoe sh. 31, 115409 Moscow, Russia; e-mail: vitali.kononenko@nsc.gpi.ru;
E.V. Bushuev A.M. Prokhorov General Physics Institute, Russian Academy of Sciences, ul. Vavilova 38, 119991 Moscow, Russia;
P.V. Volkov, A.Yu. Luk'yanov Institute for Physics of Microstructures, Russian Academy of Sciences, Akademicheskaya ul. 7, 603087 der. Afonino, Kstovskii raion, Nizhnii Novgorod region, Russia

Received 1 September 2017
Kvantovaya Elektronika **47** (11) 1012–1016 (2017)
Translated by O.M. Tsarev

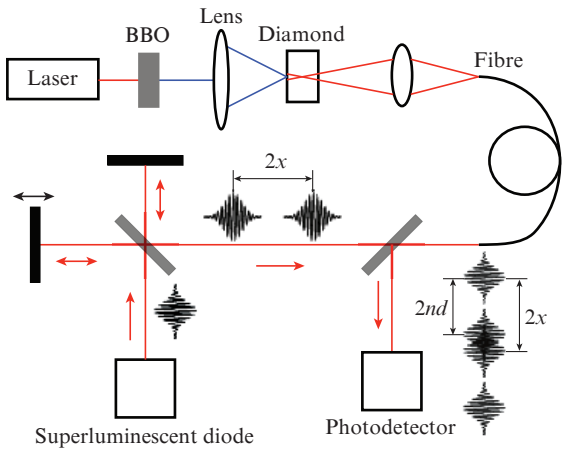

Figure 1. Experimental setup for controlled laser processing of diamond plates.

In our experiments, we used optically transparent plates of single-crystal diamond grown by plasma deposition. The plates ranged in thickness from 500 to 700 μm. After abrasive polishing on both sides, the surface roughness of the samples was 2–3 nm. The system ensured control over the translation of the sample and concurrent irradiation with a required number of laser pulses.

The operation of the system used for monitoring the thickness of transparent plates relies on low-coherence tandem interferometry, a well-known method (see e.g. the review in Ref. [20]). The probe beam of a low-coherence interferometer was combined with a processing laser beam on the surface to be processed, which allowed us to directly assess local changes in the thickness of the sample during multipulse laser irradiation. The low-coherence light source used was a superluminescent diode emitting at $\lambda = 1556$ nm. The light bandwidth was ~60 nm and the coherence length was about 20 μm. The system has the form of two sequentially optically coupled interferometers one of which (Michelson interferometer) allows the arm length difference to be tuned in a controlled way and the other is the subject of measurement (quasi-plane-parallel diamond plate). The thickness of the sample was measured on the unprocessed side (Fig. 1), which allowed us to exclude the effect of the opaque graphite-like layer formed during ablation.

The method used to measure the thickness of a transparent object builds on the fact that, in the case of partially coherent light beams, interference is only possible when the optical path difference between the beams does not exceed a certain value, a so-called coherence length of the light source. Interference at the output was observed only when the arm length differences of the two interferometers differed by less than the source coherence length, i.e. when the condition $|L_2 - L_1| < L_{coh}$ was met, where L_1 and L_2 are the arm length differences of the former and latter interferometers.

The light from the superluminescent diode was split in the tunable interferometer into two beams with an optical path difference $2x$. When reflected from the sample, each beam was again split into two, and thus four beams arrived at the photodetector (Fig. 1). In such a case, an interference pattern on the photodetector can be produced either at zero arm length difference of the tunable interferometer or when the arm length difference of the interferometer is twice the optical thickness of the plate, $2nd$ (where n is its refractive index and d is its thickness). Thus, measuring the optical thickness of the sample reduces to varying the arm length difference of the interferometer and finding the position of the maximum in the envelope of the interference signal (interference peak) coming from the photodiode. The reference interferometer and sample were optically coupled by an optical fibre, and the light was focused onto the sample by an objective. The technique was described in greater detail elsewhere [19, 21, 22].

As a reference for obtaining data on the depth of ablation and nanoablation craters produced by a preset number of laser pulses and characterised by real-time in situ measurements, we used a NewView 5000 interference surface profiler (Zygo Corp.). After laser processing, the surface topography in the irradiated zone and around it was reconstructed ex situ with nanometre accuracy using the profiler.

3. Results and discussion

3.1. Ablation

Diamond was exposed to KrF excimer laser pulses at a pulse energy of 55 mJ and fluence of 17 J cm^{-2}. During laser ablation, the interference signal gradually decreased, so that after ~20 pulses it was impossible to evaluate the thickness of the sample at the point in question. The irradiation was then stopped and the crater depth D was measured with the profiler.

Figure 2 shows a characteristic surface topography after laser irradiation, illustrating the ablation process. The gradual reduction in the visibility of the interference pattern is most likely caused by the degradation of the conditions of reflection from the crater bottom. It is seen that the nonflatness of the entire crater bottom reaches almost 2 μm. The depth difference within the low-coherence light spot is smaller: ~1 μm. However, even at this difference, the phase shift of the wavefront in the reflected beam considerably exceeds the wavelength. The fact that sample thickness measurements under such conditions yielded adequate results can be accounted for under the assumption that the interference signal is contributed predominantly by the central part of the beam, whereas its 'wings' do not arrive at the aperture of the objective because of the tilt of the crater bottom (Fig. 2). This assumption is supported by the fact that the tandem interferometry data are in excellent agreement with the surface profile depth in the central part of the crater.

Note that, according to the measurement results, the etch depth is a strictly linear function of the number of laser pulses: the mean deviation of the data points from the best fit straight line is ~10 nm (Fig. 3). The slope of the graph of the crater depth against the number of pulses determines the average material removal rate in steady-state etching mode. In the conditions under consideration, it was 210 ± 10 nm per pulse, i.e. the relative deviation of the diamond ablation rate from its average did not exceed 5%. This corresponds to fluctuations in the energy of an individual pulse, which is also ~5%.

Note also the distinct characteristic feature of the first laser pulse, which produces a crater whose depth is considerably smaller than its increase as a result of each subsequent pulse. Under the experimental conditions of this study, the difference is ~100 nm (Fig. 3, inset). This feature is due to the absence of the graphitised surface layer produced by the first

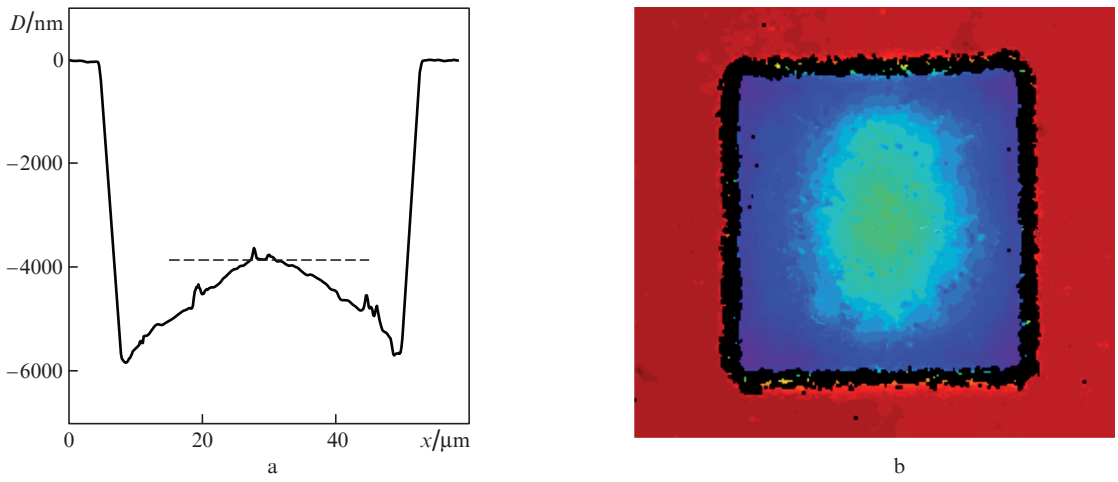

Figure 2. (Colour online) Surface (a) profile and (b) topography of a diamond plate after laser irradiation in the ablation regime (solid line). The dashed line shows the etch depth obtained from sample thickness measurements by low-coherence interferometry.

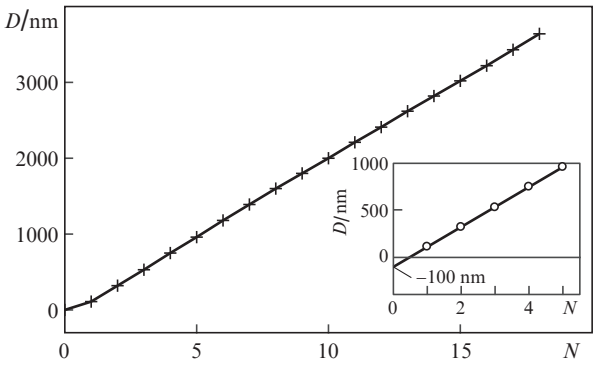

Figure 3. Ablation crater depth as a function of the number of laser pulses, N, according to sample thickness measurements by low-coherence interferometry. The inset illustrates the special feature of the ablation of diamond by the first pulse in a train.

pulse. As a result, the absorption of light and the associated heating of the material during the first pulse are substantially weaker, resulting in a smaller amount of evaporated material.

3.2. Nanoablation

The nanoablation etching of diamond was performed at a laser fluence 10% below the multipulse graphitisation threshold [23]. The irradiation procedure comprised seven series differing in the number of pulses. During each series, we collected data on the thickness of the plate in the irradiation zone. The craters thus produced, whose topology is exemplified in Fig. 4, were no more than 200 nm in depth. Thus, *in situ* (low-coherence interferometry) and *ex situ* (optical profilometry) data were compared not only for the highest irradiation fluence, as in the case of evaporative ablation, but also for intermediate fluences.

Figure 5 shows the thickness of a diamond plate as a function of the number of pulses. For clarity, the data sets are displaced by 4 nm relative to each other. Actually, the initial thicknesses at different points on the surface differed by ~100 nm, which was due to the nonflatness of the sample. Note that, without irradiation, the scatter in sequential thickness values was ~2 nm and was determined predominantly by the accuracy in digitising the interference signal. The present data demonstrate that irradiation reduces the

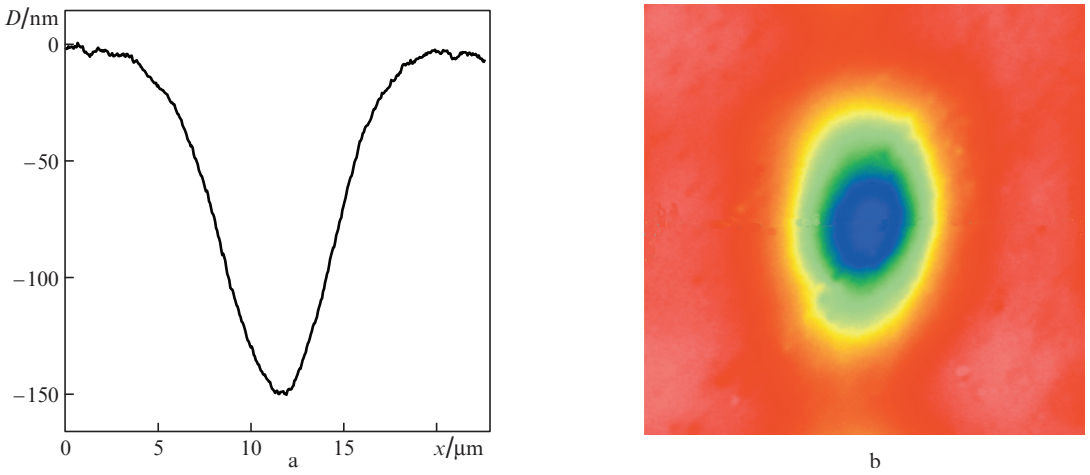

Figure 4. (Colour online) Surface (a) profile and (b) topography of a diamond plate after laser irradiation in the nanoablation regime.

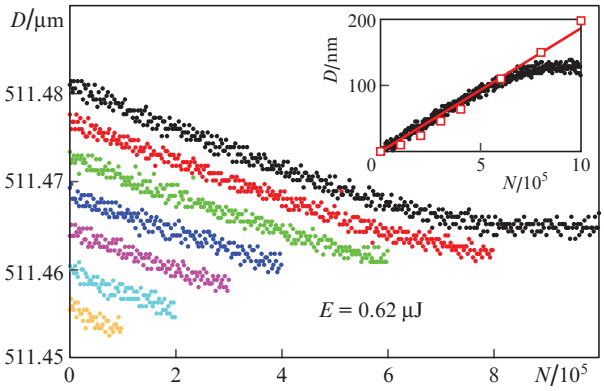

Figure 5. Reduction in the thickness of a diamond plate as a result of the nanoablation of its surface for different irradiation series (see text for more details). Inset: nanoablation crater depth as a function of the number of pulses; data obtained *in situ* using low-coherence interferometry (filled circles) and *ex situ* using an optical profiler (open squares).

sample thickness (produces a crater) and that the decrease is a linear function of the number of pulses. This correlation allows the etch depth to be determined with subnanometre accuracy via the real time averaging of the noise in individual measurements.

There are, however, two problems. First, even though the initial sample thickness (~510 μm) was measured properly, the calculated crater depths were several times smaller than those obtained in the *ex situ* measurements. The inset in Fig. 5 presents the optical profilometry and low-coherence interferometry data. The latter values are increased by a factor $K = 8$. With this correction, there is good agreement between the results obtained by the two methods. Note that, at a small crater depth, the results of the *in situ* measurements are even closer to the expected linear dependence, because they are performed at one point of the sample, whereas the *ex situ* measurements were made at different points. The other problem is that the indicated linearity is disturbed when the crater depth reaches ~100 nm.

In our opinion, both artefacts are due to the size mismatch between the etching and measurement zones. As mentioned above, the plates ranged in thickness from 500 to 700 μm. Under these conditions, to ensure equivalent conditions of probe beam reflection from both diamond surfaces, the focal length of the objective was 240 mm. The spot size was then ~30 μm, i.e. smaller than the processing zone size in the ablation regime (~40 μm) and greater than that in the nanoablation regime (~10 μm). In the described experiments, the nanoablation zone size could not be increased: the limiting factor was the pulse energy of the third harmonic, which was used to irradiate diamond.

As a result, the interference signal was divided into two components, reflected from the irradiated and unirradiated surface areas. The envelope of the former component was shifted by etching, whereas that of the latter was not. The overall envelope was also shifted, but considerably more slowly. To a first approximation, the shift decreased as the ratio of the intensity of the wanted signal (reflected from the crater) to the total intensity of the reflected signal. This ratio is easy to estimate from the ratio of the area of the etch zone to that of the zone exposed to low-coherence light. We obtain $(30\ \mu m/10\ \mu m)^2 = 9$, in agreement with the coefficient $K = 8$ chosen so as to match the *in situ* and *ex situ* measurement results.

The saturation of the etch depth is also due to the fact that the measurement zone size is too large. With increasing nanoablation crater depth, the slope of the crater wall increases. Moreover, as mentioned above, some of the reflected light becomes lost, and it is the wanted signal which is lost, whereas the signal reflected from the unirradiated zone remains unchanged. The decrease in the fraction of the wanted signal in turn leads to an increase in the coefficient K and a nonlinear variation of the crater depth with the number of pulses.

4. Conclusions

The present results demonstrate the feasibility of using low-coherence interferometry for local noncontact measurements of the optical thickness of single-crystal diamond plates and for the precision online monitoring of the laser etching of the plates, e.g. in the fabrication of diffractive optics and nanophotonic components. It has been shown that this method can be used for monitoring the laser structuring of diamond surfaces in both laser irradiation regimes: evaporative ablation and photostimulated nanoablation. The accuracy achieved in real-time measurements of the depth of a reproducible surface topography is 10 nm or better, which paves the way to the automation of laser profiling processes, as well as of micro- and nanostructuring of transparent superhard materials.

Acknowledgements. This work was supported by the Russian Science Foundation (Project No. 14-22-00243).

References

1. Kononenko V.V., Kononenko T.V., Konov V.I., Pimenov S.M., Garnov S.V., Tishchenko A.V., Prokhorov A.M., Khomich A.V. *Quantum Electron.*, **29** (2), 158 (1999) [*Kvantovaya Elektron.*, **26** (2), 158 (1999)].
2. Kononenko V.V., Konov V.I., Pimenov S.M., Prokhorov A.M., Pavel'ev V.S., Soifer V.A. *Quantum Electron.*, **29** (1), 9 (1999) [*Kvantovaya Elektron.*, **26** (1), 9 (1999)].
3. Lee K.G., Chen X.W., Eghlidi H., Kukura P., Lettow R., Renn A., Sandoghdar V., Gotzinger S. *Nat. Photonics*, **5**, 166 (2011).
4. Castelletto S., Harrison J.P., Marseglia L., Stanley-Clarke A.C., Gibson B.C., Fairchild B.A., Hadden J.P., Ho Y.-L.D., Hiscocks M.P., Ganesan K., Huntington S.T., Ladouceur F., Greentree A.D., Prawer S., O'Brien J.L., Rarity J.G. *New J. Phys.*, **13**, 025020 (2011).
5. Sotillo B., Bharadwaj V., Hadden J.P., Sakakura M., Chiappini A., Fernandez T.T., Longhi S., Jedrkiewicz O., Shimotsuma Y., Criante L., Osellame R., Galzerano G., Ferrari M., Miura K., Ramponi R., Barclay P.E., Eaton S.M. *Sci. Rep.*, **6**, 052330 (2016).
6. Wrachtrup J., Jelezko F. *J. Phys.: Condens. Matter*, **18**, S807 (2006).
7. Kurtsiefer C., Mayer S., Zarda P., Weinfurter H. *Phys. Rev. Lett.*, **85**, 290 (2000).
8. Neumann P., Beck J., Steiner M., Rempp F., Fedder H., Hemmer P.R., Wrachtrup J., Jelezko F. *Science*, **329**, 542 (2010).
9. Siyushev P., Pinto H., Voros M., Gali A., Jelezko F., Wrachtrup J. *Phys. Rev. Lett.*, **110**, 167402 (2013).
10. Aharonovich I., Greentree A.D., Prawer S. *Nat. Photonics*, **5**, 397 (2011).
11. Rothschild M., Arnone C., Ehrlich D.J. *J. Vac. Sci. Technol. B*, **4**, 310 (1986).
12. Konov V.I., Pimenov S.M., Prokhorov A.M., Smolin A.A., Chapliev N.I. *Sov. J. Quantum Electron.*, **21** (9), 993 (1991) [*Kvantovaya Elektron.*, **18** (9), 1096 (1991)].
13. Preuss S., Stuke M. *Appl. Phys. Lett.*, **67**, 338 (1995).
14. Kononenko V.V., Kononenko T.V., Pimenov S.M., Sinyavskii M.N., Konov V.I., Dausinger F. *Quantum Electron.*, **35** (3), 252 (2005) [*Kvantovaya Elektron.*, **35** (3), 252 (2005)].

15. Shinoda M., Gattass R.R., Mazur E. *J. Appl. Phys*., **105**, 053102 (2009).
16. Kononenko V.V., Komlenok M.S., Pimenov S.M., Konov V.I. *Quantum Electron*., **37** (11), 1043 (2007) [*Kvantovaya Elektron*., **37** (11), 1043 (2007)].
17. Gololobov V.M., Kononenko V.V., Konov V.I. *Quantum Electron*., **46** (12), 1154 (2016) [*Kvantovaya Elektron*., **46** (12), 1154 (2016)].
18. Kononenko V.V., Vlasov I.I., Gololobov V.M., Kononenko T.V., Semenov T.A., Khomich A.A., Shershulin V.A., Krivobok V.S., Konov V.I. *Appl. Phys. Lett*., **111**, 081101 (2017).
19. Kononenko V.V., Konov V.I., Pimenov S.M., Volkov P.V., Goryunov A.V., Ivanov V.V., Novikov M.A., Markelov V.A., Tertyshnik A.D., Ustavshchikov S.S. *Quantum Electron*., **35** (7), 622 (2005) [*Kvantovaya Elektron*., **35** (7), 622 (2005)].
20. Rao Y.-J., Jackson D.A. *Meas. Sci. Technol*., **7**, 981 (1996).
21. Volkov P.V., Goryunov A.V., Daniltsev V.M., Luk'yanov A.Y., Pryakhin D.A., Tertyshnik A.D., Khrykin O.I., Shashkin V.I. *J. Cryst. Growth*, **310**, 4724 (2008).
22. Bushuev E.V., Yurov V.Y., Bolshakov A.P., Ralchenko V.G., Ashkinazi E.E., Ryabova A.V., Antonova I.A., Volkov P.V., Goryunov A.V., Luk'yanov A.Y. *Diamond Relat. Mater*., **66**, 83 (2016).
23. Kononenko V.V., Gololobov V.M., Konov V.I. *Appl. Phys. A*, **122**, 1 (2016).